Neonatal cardiomyopathy in mice homozygous for the Arg403Gln mutation in the α cardiac myosin heavy chain gene

Diane Fatkin,[1] Michael E. Christe,[2] Orlando Aristizabal,[3] Bradley K. McConnell,[2] Shardha Srinivasan,[3] Frederick J. Schoen,[4] Christine E. Seidman,[1] Daniel H. Turnbull,[3] and J.G. Seidman[2]

[1]Cardiovascular Division and Howard Hughes Medical Institute, Brigham and Women's Hospital, Boston, Massachusetts 02115, USA
[2]Department of Genetics, Howard Hughes Medical Institute and Harvard Medical School, Boston, Massachusetts 02115, USA
[3]Skirball Institute of Biomolecular Medicine, New York University Medical Center, New York, New York 10016, USA
[4]Department of Pathology, Brigham and Women's Hospital and Harvard Medical School, Boston, Massachusetts 02115, USA

Address correspondence to: J.G. Seidman, Department of Genetics, Harvard Medical School, Alpert Building, 200 Longwood Avenue, Boston, Massachusetts 02115, USA. Phone: (617) 432-7871; Fax: (617) 432-7832; E-mail: Seidman @rascal.med.harvard.edu

Received for publication July 17, 1998, and accepted in revised form November 6, 1998.

Heterozygous mice bearing an Arg403Gln missense mutation in the α cardiac myosin heavy chain gene (α-MHC$^{403/+}$) exhibit the histopathologic features of human familial hypertrophic cardiomyopathy. Surprisingly, homozygous α-MHC$^{403/403}$ mice die by postnatal day 8. Here we report that neonatal lethality is caused by a fulminant dilated cardiomyopathy characterized by myocyte dysfunction and loss. Heart tissues from neonatal wild-type and α-MHC$^{403/403}$ mice demonstrate equivalent switching of MHC isoforms; α isoforms in each increase from 30% at birth to 70% by day 6. Cardiac dimensions and function, studied for the first time in neonatal mice by high frequency (45 MHz) echocardiography, were normal at birth. Between days 4 and 6, α-MHC$^{403/403}$ mice developed a rapidly progressive cardiomyopathy with left ventricular dilation, wall thinning, and reduced systolic contraction. Histopathology revealed myocardial necrosis with dystrophic calcification. Electron microscopy showed normal architecture intermixed with focal myofibrillar disarray. We conclude that 45-MHz echocardiography is an excellent tool for assessing cardiac physiology in neonatal mice and that the concentration of Gln403 α cardiac MHC in myocytes influences both cell function and cell viability. We speculate that variable incorporation of mutant and normal MHC into sarcomeres of heterozygotes may account for focal myocyte death in familial hypertrophic cardiomyopathy.

J. Clin. Invest. **103**:147–153 (1999).

Introduction

Familial hypertrophic cardiomyopathy (FHC) is inherited as an autosomal dominant trait that is characterized by unexplained hypertrophy of the ventricular myocardium with histologic evidence of myocyte and myofibrillar disarray. Myocyte loss and replacement fibrosis are often prominent features, which can contribute to arrhythmias and altered myocardial hemodynamics in FHC. Molecular genetic studies have demonstrated that FHC is caused by mutations in genes encoding cardiac sarcomere proteins; these defects are most commonly found in the β cardiac myosin heavy chain (MHC) gene (1, 2). The mechanism(s) by which mutated sarcomere proteins cause the clinical features of FHC is largely unknown.

We have developed a mouse model for FHC by introducing a missense mutation identified in humans (β cardiac MHC Arg403Gln; ref. 1) into the murine α cardiac MHC gene using homologous recombination (3). In humans, the Arg403Gln mutation causes marked histopathology, ventricular dysfunction, and a high incidence of sudden death (4). Heterozygous α cardiac MHC mutant mice (α-MHC$^{403/+}$) develop myocardial histologic abnormalities similar to human FHC by 15 weeks of age. Sedentary α-MHC$^{403/+}$ mice have a normal life span. Homozygous α cardiac MHC mice (α-MHC$^{403/403}$) were generated to examine the consequences of complete replacement of normal myosin by mutant peptide. α-MHC$^{403/403}$ pups were liveborn, but, unlike their heterozygous littermates, they all died within one week.

We report studies of cardiac structure and function in normal and α-MHC$^{403/403}$ mice using a new high-frequency (45 MHz) echocardiographic technique (5, 6). Our data provide the first demonstration that high-quality images can be obtained by 45-MHz echocardiography for *in vivo* assessment of myocardial size and contractility in neonatal mice. Markedly abnormal physiology and pathology were found in α-MHC$^{403/403}$ hearts. These data explain the neonatal lethality of homozygous mutants and provide insights into a potential etiology for myocyte death in human FHC.

Methods

Animals. Details of the targeting construct and homologous recombination procedures used in the generation of α-MHC$^{403/+}$ mice have been described previously (3). α-MHC$^{403/403}$, α-

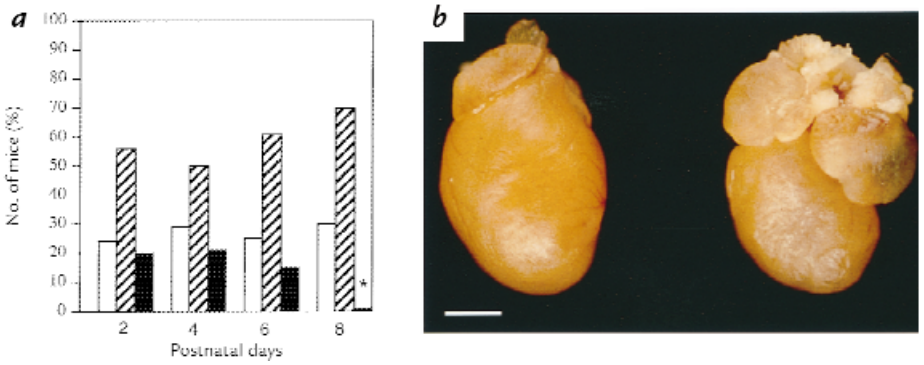

Figure 1
(***a***) Relative proportions of wild-type mice (*open bars*), α-MHC$^{403/+}$ mice (*hatched bars*), and α-MHC$^{403/403}$ mice (*filled bars*) alive at postnatal days 2, 4, 6, and 8. The asterisk represents significant difference between observed and expected proportions of α-MHC$^{403/403}$ mice; $P < 0.001$. (***b***) Hearts from a postnatal day 6 wild-type mouse (*left*) and an α-MHC$^{403/403}$ mouse (*right*). Dilation of both atria is present in the α-MHC$^{403/403}$ mouse heart. Scale bar, 1 mm. *MHC,* myosin heavy chain.

MHC$^{403/+}$, and wild-type (strain 129/Black Swiss) mice were studied between postnatal day 0 (birth) and day 6. Mouse genotype was determined by restriction enzyme digestion of PCR-amplified tail DNA (3). All mice were maintained according to protocols approved by the Institutional Animal Care and Use Committees of Harvard Medical School and New York University Medical Center.

Pathology. Fixed hearts were examined grossly and then bisected transversely at the midventricular level before histologic examination. Both apical and basal halves were embedded in paraffin or glycol methacrylate plastic (JB-4; Polysciences Inc., Warrington, Pennsylvania, USA), sectioned from the cut surfaces at ~5 μm and 2 μm, respectively, and stained for light microscopy with hematoxylin and eosin (for overall morphology). Selected paraffin sections were also stained with Masson's trichrome stain (for collagen) and Von Kossa's reagent (for calcium phosphates). Myocardial necrosis and calcification were graded as follows: 0, not present; 1+, mild, comprising a single small focus of necrosis and/or calcification; 2+, moderate, multifocal-to-confluent foci; and 3+, severe, large, confluent clusters and/or transmural involvement. Histologic specimens were further counterstained with methyl green for morphologic analysis of myocyte nuclei.

Myocardial tissue processed for transmission electron microscopy was fixed in 2.5% glutaraldehyde and 2.0% paraformaldehyde in cacodylate buffer at pH 7.4, postfixed in 2.0% osmium tetroxide, dehydrated in ethanol in propylene oxide, and embedded in Poly/Bed 812 (Polysciences Inc.). Sections were cut at 60 nM, stained with lead citrate and uranyl acetate, and examined with a JEOL-100CX transmission electron microscope (JEOL USA Inc., Cranford, New Jersey, USA) at an accelerating voltage of 80 kV.

Echocardiography. Transthoracic echocardiography was performed without anesthesia and with mice lightly restrained in a supine position, at ambient temperatures >25°C, using a Humphrey Ultrasound Biomicroscope (model 840; Humphrey Instruments, San Leandro, California, USA). Two-dimensional images were obtained using a mechanically scanned, focused transducer (gently positioned over a layer of acoustic gel on the anterior chest to avoid pressure that might cause bradycardia) that operated at a nominal frequency of 45 MHz. The spatial resolution of the echocardiographic system was 30 μm in the axial (depth) direction and 65 μm in the lateral (horizontal) direction; penetration depth was 4–5 mm. Two-dimensional 5 × 5-mm, 8-bit grayscale video images were acquired at a scan rate of 8 Hz, with a gain setting of 80 dB and a time gain correction of 5 dB/mm.

Continuous-wave Doppler. Continuous-wave (CW) Doppler interrogation was performed immediately after two-dimensional echocardiographic imaging. The CW Doppler probe was manipulated at a constant angle on the left anterior chest wall until maximal blood velocity signals were obtained. A high-frequency Doppler ultrasound system using two air-backed lithium niobate transducers operating at an ultrasound frequency of 43 MHz (6) was used. The two transducers were aligned to obtain overlapping ultrasound beams (angle of intersection is 30°), the intersection of which defines the Doppler sample volume. Transducers were fabricated with diameters between 1 and 1.5 mm, resulting in Doppler sample volumes between 0.5 and 1.5 mm^3. CW Doppler data were recorded onto digital audio tapes and analyzed on a PC computer in the form of a spectrogram (6). Conversion between Doppler shift frequency and blood velocity was made assuming a speed of sound in blood of 1,580 m/s (7) to obtain a conversion factor of 0.02 (mm/s)/Hz.

Table 1
Echocardiographic data for wild-type (+/+), heterozygous (403/+), and homozygous (403/403) α cardiac MHC mutant mice on postnatal days 0, 4, and 6

	Mouse genotype			
	+/+	403/+	403/403	*P* value
Day 0	(*n* = 6)	(*n* = 15)	(*n* = 9)	
Weight (g)	1.38 ± 0.23	1.45 ± 0.22	1.28 ± 0.20	NS
Heart rate (bpm)	268 ± 54	257 ± 28	245 ± 50	NS
LVDD (mm)	1.37 ± 0.08	1.31 ± 0.09	1.28 ± 0.09	NS
LVSD (mm)	0.91 ± 0.08	0.83 ± 0.07	0.82 ± 0.08	NS
LVFS (%)	34 ± 4	36 ± 4	36 ± 4	NS
LVWT (mm)	0.21 ± 0.02	0.20 ± 0.03	0.19 ± 0.02	NS
Day 4	(*n* = 4)	(*n* = 13)	(*n* = 7)	
Weight (g)	2.37 ± 0.52	2.15 ± 0.51	2.35 ± 0.50	NS
Heart rate (bpm)	314 ± 49	273 ± 50	288 ± 50	NS
LVDD (mm)	1.66 ± 0.17	1.55 ± 0.16	1.91 ± 0.20	<0.001
LVSD (mm)	0.98 ± 0.10	0.93 ± 0.11	1.29 ± 0.32	0.003
LVFS (%)	41 ± 6	39 ± 6	33 ± 11	NS
LVWT (mm)	0.21 ± 0.03	0.20 ± 0.02	0.16 ± 0.03	0.024
Day 6	(*n* = 11)	(*n* = 26)	(*n* = 6)	
Weight (g)	3.34 ± 0.83	3.79 ± 0.76	3.35 ± 0.76	NS
Heart rate (bpm)	304 ± 41	287 ± 53	244 ± 34	NS
LVDD (mm)	1.78 ± 0.26	1.72 ± 0.19	1.90 ± 0.22	NS
LVSD (mm)	0.98 ± 0.18	0.93 ± 0.15	1.28 ± 0.28	<0.001
LVFS (%)	45 ± 8	45 ± 8	33 ± 11	0.006
LVWT (mm)	0.28 ± 0.05	0.27 ± 0.03	0.21 ± 0.04	0.003

Abbreviations as explained in text.

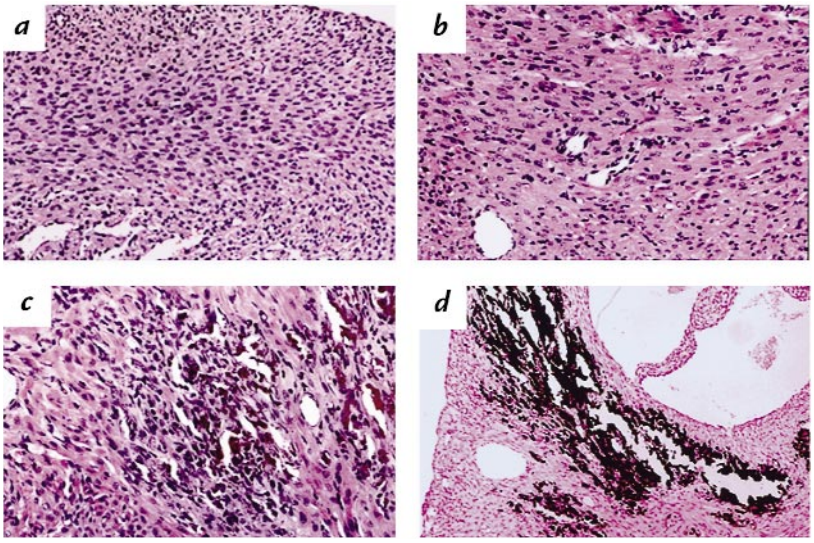

Figure 2
Myocardial histology in α-MHC$^{403/403}$ mice. (***a***) Normal cardiac structure at postnatal day 0. (***b–d***) Myocardial abnormalities observed in all α-MHC$^{403/403}$ mice at postnatal day 6: (*b*) mild myocyte hypertrophy, (*c*) characteristic lesion with well-established necrosis, (*d*) dystrophic calcification at sites of focal myocardial necrosis. Sections stained with hematoxylin and eosin (*a–c*) or Von Kossa's stain (*d*). *a*, ×190; *b*, ×190; *c*, ×110; *d*, ×45.

Data analysis. Left ventricular (LV) diameters, areas, and wall thicknesses were obtained from cross-sectional short-axis views. Diastolic and systolic LV dimensions were measured from six consecutive cardiac cycles. To account for the low frame rates and lack of synchronization of image acquisition with the cardiac cycle, LV diastolic diameter (LVDD) was calculated from the mean of the three maximal diastolic measurements; LV systolic diameter (LVSD) was calculated from the mean of the three minimal systolic measurements. Left ventricular wall thickness (LVWT) was derived from the mean of three minimum diastolic wall thickness measurements. The coefficient of variation for each set of measurements was expressed as the SD/mean. Left ventricular fractional shortening (LVFS) was expressed as a percentage, using the formula (LVDD – LVSD) / LVDD × 100. Heart rates were calculated using the time interval between successive waveforms on CW Doppler tracings. Measurements were made without prior knowledge of genotype. Inter- and intraobserver variability was assessed by comparison of independent measurements of LV dimensions by two observers, and on two different occasions, by one observer.

Protein assays. α-MHC$^{403/403}$ and wild-type mouse hearts were harvested at postnatal days 0, 2, 4, and 6. Ventricles were isolated, washed in PBS, blotted on filter paper, and immediately frozen in liquid N_2. Tissues were homogenized in 1 ml of ice-cold inhibiting buffer (8) containing 50 mM KH_2PO_4, 70 mM NaF, and 5 mM EDTA, with protease inhibitors (5 μg/ml antipain, 10 μg/ml leupeptin, 5 μg/ml pepstatin A, 43 μg/ml phenylmethylsulfonyl fluoride, 5 mM EGTA, and 0.1 μM sodium orthovanadate), and centrifuged at 15,000 *g* for 5 min at 4°C. The pellet was incubated on ice for 30 min in inhibiting buffer plus 1% Triton X-100 plus protease inhibitors, and then centrifuged at 5,000 *g* for 5 min. Detergent-extracted myofibrils were resuspended in inhibiting buffers.

Myofibrillar proteins were separated by SDS-PAGE. Proteins were solubilized and denatured in sample preparation buffer containing 4% SDS, 0.23 M β-mercaptoethanol, and 0.2 M Tris-HCl (pH 6.5) at 100°C for 5 min. Protein concentration was determined using the Bradford protein assay. Proteins were separated by PAGE in the presence of 0.1% SDS at constant current (50 mA, for 30 h) on 6% polyacrylamide gels with recirculated, cooled (15°C) running buffers. After electrophoresis, the gels were silver-stained and dried. The relative proportions of α and β cardiac MHC isoforms and a high molecular weight protein reference standard were quantified using densitometry.

Statistical analysis. The significance of differences in survival of α-MHC$^{403/403}$, α-MHC$^{403/+}$, and wild-type mice was assessed by the one-group χ^2 test. Echocardiographic measurements made in the three groups of mice were compared by one-factor ANOVA and Student's *t* test. Relationships between continuous variables were characterized using linear regression analysis. Comparison of inter- and intraobserver measurements were determined using linear regression analysis and Bland and Altman's "limits of agreement" (9), in which acceptable reproducibility requires ≥ 95% of the data to be within ± 2 SD of the mean difference. Data are expressed as mean ± SD. $P < 0.05$ was considered significant.

Results

Survival analysis. MHC$^{403/403}$ mice were produced by mating heterozygous α-MHC$^{403/+}$ mice. At birth, the ratio of α-MHC$^{403/403}$/α-MHC$^{403/+}$/wild-type mice approximated

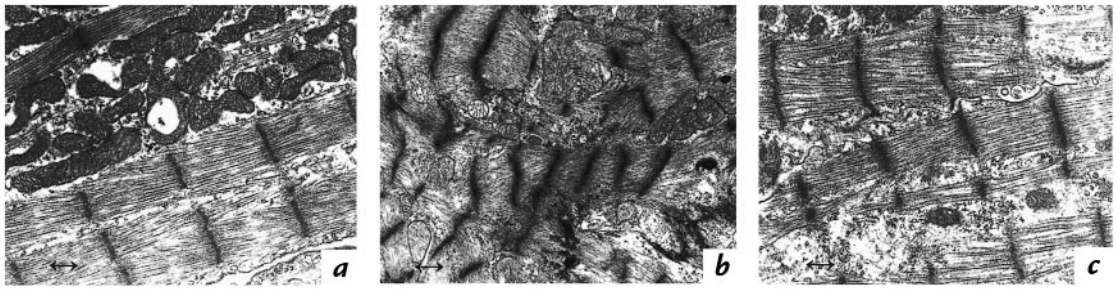

Figure 3
Electron microscopy of cardiac myofibrils at postnatal day 6 in an α-MHC$^{403/403}$ mouse (***a*** and ***b***) and a wild-type mouse (***c***). Regions of relatively preserved sarcomere assembly (*a*) and myofiber disarray (*b*) present in the α-MHC$^{403/403}$ mouse heart. Marker length, 0.4 μm.

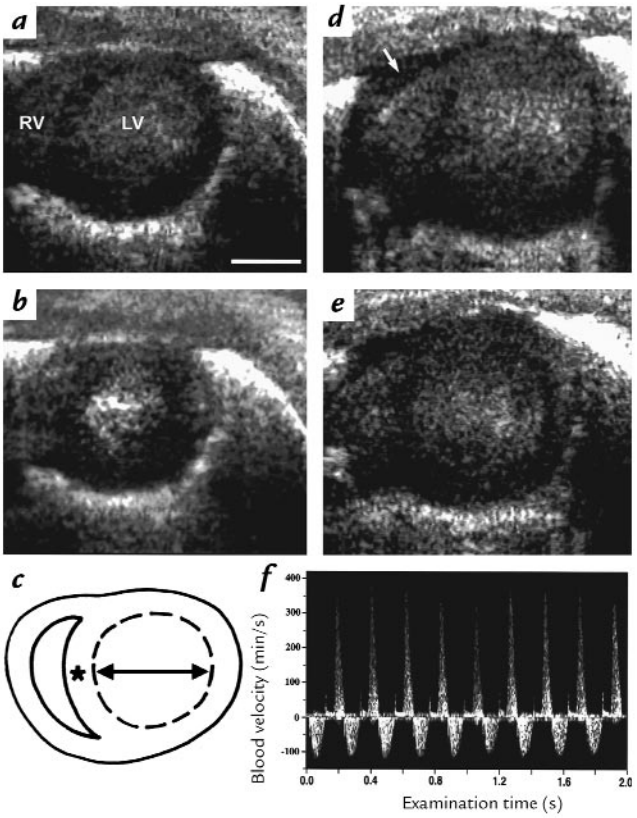

Figure 4

Two-dimensional images obtained by 45-MHz echocardiography demonstrating the left ventricle (*LV*) and right ventricle (*RV*) in a short-axis view in diastole (***a*** and ***d***) and systole (***b*** and ***e***). Normal cardiac size and function at postnatal day 6 in a α-MHC$^{403/+}$ mouse (***a*** and ***b***). The LV is dilated and thin-walled with reduced systolic contraction in an α-MHC$^{403/403}$ mouse (***d*** and ***e***). In addition, RV dilation, LA dilation, and a pericardial effusion (*d, arrow*) were identified. Echocardiographic measurements (***c***) were as follows: transverse LV diameter (*arrow*), LV area (*dashed lines*), and LV wall thickness (*asterisk*). (***f***) Bidirectional blood flow velocity pattern on CW Doppler interrogation of the left hemithorax, consistent with transmitral LV inflow (positive velocity) and aortic outflow (negative velocity). Scale bar, 1 mm. *LV* left ventrical; *RV* right ventrical; *LA*, left atrium.

the expected ratios of 1:2:1. After postnatal day 5, survival of α-MHC$^{403/403}$ mice decreased progressively (Fig. 1*a*); none lived beyond postnatal day 8.

Cardiac pathology. Hearts from wild-type and α-MHC$^{403/+}$ mice had normal structure and histology at postnatal days 0–6 (data not shown). Mitoses of cardiac myocytes were frequent in hearts of one-day-old animals but rarely noted thereafter. Gross examination of α-MHC$^{403/403}$ mouse hearts revealed LV dilation and discoloration, with enlargement of the left and right atrium (LA, RA, respectively) (Fig. 1*b*). Myocardial histology and prevalence of mitoses in α-MHC$^{403/403}$ mice were normal at day 0. By postnatal day 2, histopathology was present, and it increased in frequency and severity with age (Fig. 2 and data not shown). Pathologic findings predominated in the LV free wall and interventricular septum. There was diffuse mild-to-moderate myocyte hypertrophy accompanied by lesions of focal necrosis involving several contiguous myocytes or multifocal, confluent, and transmural necrosis. This distinctive pattern of injury occurred without inflammation but often was accompanied by secondary dystrophic calcification (Fig. 2*d*). By postnatal day 6, myocardial necrosis was present in 100% (n = 15) of α-MHC$^{403/403}$ mice; in 14 animals, this was moderate to severe (grades 2+/3+). Dystrophic calcification was present in 87% (n = 13); in nine hearts, this was moderate to severe. No mice had calcification in the absence of necrosis.

Electron microscopy of α-MHC$^{403/403}$ hearts demonstrated normal sarcomere structure (Fig. 3), with alignment of myofibrils along the long axis of the myocytes and the presence of intact Z bands throughout the cell length. Although some sections showed focal myofibrillar disarray, most were indistinguishable from sections derived from α-MHC$^{403/+}$ or wild-type mice.

Echocardiographic studies were performed in 97 mice between ages 0 and 6 days without procedural complications or deaths. Image acquisition was completed on each mouse within 10–15 minutes. Cross-sectional LV images were obtained in a short-axis view in each animal. The right ventricle (RV) was visualized in the majority of studies. The LA was observed only when pathological dilation was present; the RA was not observed in any study.

Good correlations were obtained between two observers for LV cavity dimensions: LVDD (r = 0.88, P < 0.001), LV diastolic area (LVDA, r = 0.85, P < 0.001), LVSD (r = 0.61, P < 0.001), LV systolic area (LVSA, r = 0.55, P < 0.001), LVFS (r = 0.74, P < 0.001). Left ventricular wall thickness measurements demonstrated greater interobserver variability (r = 0.30, P = 0.007) than did LV diameters and areas. Intraobserver correlations for all LV parameters were high: LVDD (r = 0.98, P < 0.001), LVDA (r = 0.98, P < 0.001), LVSD (r = 0.97, P < 0.001), LVSA (r = 0.96, P < 0.001), LVFS (r = 0.96, P < 0.001), and LVWT (r = 0.50, P < 0.001). All LV parameters were within, or close to, the 95% limits of agreement (range 92%–98%). The coefficient of variation for measurements made by a single observer on one occasion was <5% for LV diameters and areas and <7% for LV wall thickness.

No significant differences were observed in cardiac morphology or size between wild-type and α-MHC$^{403/+}$ mice during days 0–6 (Table 1). Heart rates were also equivalent but notably lower (~50%) than those observed in conscious adult animals (Table 1 and data not shown).

Echocardiographic parameters of α-MHC$^{403/403}$ mouse hearts were indistinguishable from those of littermates at birth (Table 1). Increases in LV chamber dimensions (LVDD and LVSD) and LV wall thinning were evident by postnatal day 4. Contractile function was preserved in three of four α-MHC$^{403/403}$ mice but was reduced in four mice (LVFS = 19%, 23%, 26%, and 31%). These parameters tended to worsen by postnatal day 6, at which time all α-MHC$^{403/403}$ mice exhibited a global reduction of systolic contraction and/or LV dilation. Echocardiographic studies on postnatal day 6 demonstrated biventricular failure in 50% of α-MHC$^{403/403}$ mice: LA, LV, and RV dilatation and pericardial effusion (Fig. 4) were present. Echo-dense material detected in the LA of these animals was caused by thrombus in the dilated LA cavity, with foci of necrosis in the LA myocardium (Fig. 5).

The extent of myocardial necrosis in α-MHC$^{403/403}$ mouse hearts correlated with chamber dimensions and function (LVDD, P < 0.001; LVFS, P < 0.001). By postnatal

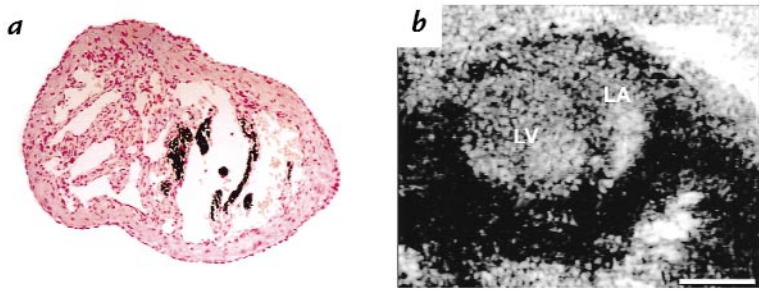

Figure 5
Left atrial pathology at postnatal day 6 in α-MHC$^{403/403}$ mice. (***a***) Cut section stained with Von Kossa's reagent shows necrosis and calcification of myocardium in the LA appendage. ×80. (***b***) Echocardiographic findings in an α-MHC$^{403/403}$ mouse with LV dilation and contractile dysfunction. Two-dimensional echocardiographic images show dense echogenicity consistent with thrombus formation in a dilated LA. Scale bar, 1 mm.

day 4, myocardial necrosis was present in all α-MHC$^{403/403}$ mice with reduced LVFS (n = 4) and in two of the three mice with normal LVFS (necrosis grades 1+ and 3+, respectively). On day 6, myocardial necrosis was present in all mice with reduced LVFS (n = 4) and in two mice with normal LVFS (necrosis grades 2+ and 3+, respectively).

Cardiac MHC isoforms. The total amount of cardiac MHC in the myofibrillar fractions was assessed by comparison to a high molecular weight protein; the total amount of cardiac MHC was the same in myofibrillar fractions from wild-type and α-MHC$^{403/403}$ mouse hearts (data not shown). Levels of α and β cardiac MHC isoforms were assessed in wild-type and α-MHC$^{403/403}$ mice hearts by sodium dodecyl sulfate-polyacrylamide gel electrophoresis (SDS-PAGE) (Fig. 6). In wild-type mice, ventricular levels of β cardiac MHC exceeded α cardiac MHC at day 0 (β = 66%, α = 34%); by day 6, the cardiac MHC isoform switch was virtually complete, with a predominance of the α isoform (β = 27%, α = 73%). This pattern of expression was not significantly altered in α-MHC$^{403/403}$ mice: day 0, β-MHC = 73%, α-MHC = 27%; day 6, β-MHC = 30%, α-MHC = 70%.

Discussion

Cardiac structure and function of neonatal α-MHC$^{403/403}$ mice demonstrate that homozygous mice bearing the Arg403Gln mutation develop a rapidly progressive, lethal cardiomyopathy. Unlike the cardiomyopathy observed in heterozygous α-MHC$^{403/+}$ mice, systolic dysfunction, myocardial necrosis, and dystrophic calcification are the predominant features of the α-MHC$^{403/403}$ pathology. These data demonstrate the technical feasibility of *in vivo* cardiac assessment of neonatal mice and indicate that myocyte dysfunction and loss may be important in the pathophysiology of human FHC.

The application of genetic engineering to study the molecular basis of cardiovascular structure and function has posed an important research challenge: assessment of cardiac physiology in small rodents. We demonstrate that 45-MHz echocardiography is a powerful tool for assessing *in vivo* cardiac function despite the extremely small size and high beating rates of neonatal mouse hearts. An important finding from these studies is a developmental profile of normal neonatal cardiac function during the first week of life. Neonatal mice had slower heart rates and reduced contractile function when compared with adult mice. Although LVFS increases (from 34% to 45%) during the first week of life, neonatal heart rates (~300 beats per minute [bpm]) remain slow. Increases in LVFS are probably due to altered cardiac MHC isoform expression that occurs in the first postnatal week (Fig. 6 and ref. 10), a hypothesis supported by previous *in vitro* and *in vivo* investigations. Myocytes expressing β cardiac MHC have lower myosin adenosine triphosphatase (ATPase) activity and lower velocity of fiber shortening than do myocytes that express α cardiac MHC (11–16). Furthermore, the LVFS values (34%–36%) observed in neonatal mice during the first few days after birth were equivalent to values reported in the embryonic mouse at E12.5–E13.5 (5) and in other species, such as humans (17–19) and rabbits (20), in which the β-MHC isoform predominates. In contrast, the LVFS observed after one week (45%) was similar to that reported previously in adult mice (21–23) and in other small rodents, such as adult rats (24), in which the α cardiac MHC isoform predominates.

Unlike wild-type and heterozygous littermates, an increase in systolic contractility did not occur in α-MHC$^{403/403}$ mouse hearts, and progressive LV dilation ensued. Given that the α/β cardiac MHC isoform ratio at postnatal day 6 in α-MHC$^{403/403}$ mice was similar to that observed in wild-type hearts, the relatively lower mean LVFS could not be attributed to failure of the β-to-α isoform switch nor to upregulation of the β isoform in response to the LV functional deficit. The myocardial contractile dysfunction observed in α-MHC$^{403/403}$ mouse

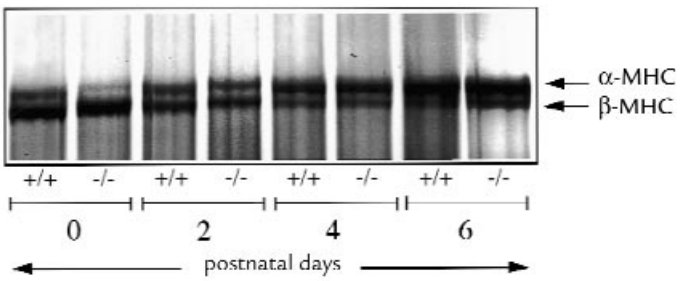

Figure 6
Silver-stained 6% SDS-polyacrylamide gel showing cardiac MHC isoforms at postnatal days 0, 2, 4, and 6 in wild-type mice and α-MHC$^{403/403}$ mice. Note the developmental changes in expression of cardiac MHC in ventricular myocardium in both groups of mice; at postnatal day 0, the β isoform (*lower molecular weight band*) is predominant, with a switch to predominance of the α isoform (*higher molecular weight band*) by postnatal day 6.

hearts is caused by the Arg403Gln mutation in α cardiac MHC. Residue 403 is situated in the head of the MHC at the base of a loop that interacts with actin (25), and *in vitro* studies (26, 27) have demonstrated the Arg403Gln substitution alters the kinetics of the actin–myosin interaction by reducing actin translocating activity and actin-associated ATPase. Reductions in actin translocation can result in a lowered force/stiffness ratio and depressed velocity of shortening (28, 29), thereby producing global contractile dysfunction and LV dilation in neonatal α-MHC$^{403/403}$ mice.

Although the mechanism by which mutant MHC produces myocyte necrosis remains to be elucidated, calcium is a likely participant. Heightened calcium sensitivity in heterozygous α-MHC$^{403/+}$ hearts (30) and prolonged calcium transients have been observed in ventricular muscle preparations from animal models and patients with FHC (31); both suggest a propensity for calcium overload. However, the gross morphologic calcification in α-MHC$^{403/403}$ heart sections (Fig. 2*d*) probably reflects a different process; its rapid appearance in preexisting necrotic foci is most consistent with accelerated dystrophic calcification (32) in young animals, in which bone mineralization mechanisms are active (33, 34). Left ventricular contractile dysfunction and dilation could promote myocardial ischemia and subsequent necrosis by reducing coronary artery perfusion, either directly through LV pump failure or indirectly through catecholamine-induced vasospasm (35). However, the distribution of necrotic lesions in α-MHC$^{403/403}$ hearts are atypical for coronary ischemia, in which pathology is positioned along vascular beds, and observed heart rates were not consistent with increased catecholamine levels.

These data have important ramifications for understanding the histopathology in human FHC. Affected individuals with this disorder are almost always heterozygous, with one mutant sarcomere protein gene allele and one normal allele (1). However, individuals with homozygous sarcomere protein gene mutations have been observed very infrequently (36, and our unpublished data). Cardiac histopathology in heterozygous individuals typically shows marked variation in the distribution and severity of findings; foci with marked myofibrillar disarray, myocyte death, and replacement fibrosis are juxtaposed to normal myocardium. On the basis of the studies of α-MHC$^{403/403}$ mice, we speculate that variable incorporation of mutant α cardiac MHC into sarcomeres may account for variability of cell viability in FHC. This is consistent with a "poison polypeptide" effect: levels above a critical threshold for mutant peptide (or sarcomere dysfunction) may cause the myocyte to die. Patchy myocyte loss probably contributes to arrhythmias in FHC; more global involvement results in the dilated phase of this disease. Myocyte loss has also been implicated in the progression of ventricular dysfunction and remodeling in cardiomyopathies associated with chronic ischemia, myocardial infarction, pressure overload hypertrophy, hypertension, chronic tachycardia, pacing, and aging (37–42). Hence, elucidation of the cellular events triggered by sarcomere dysfunction in the α-MHC$^{403/403}$ mouse should provide insights into myocyte necrosis and LV dilation in many cardiomyopathies.

Acknowledgments

This research was supported by the Howard Hughes Medical Institute and the Whitaker Foundation. We are grateful to Humphrey Instruments for the use of the ultrasound biomicroscope used in these studies. D.H. Turnbull is an Investigator of the American Heart Association/New York City affiliate. We thank Helen Shing for technical assistance with electron microscopy.

1. Seidman, C., and Seidman, J.G. 1995. Gene mutations that cause familial hypertrophic cardiomyopathy. In *Molecular cardiovascular medicine*. E. Haber, editor. Scientific American. New York, NY. 193–210.
2. Watkins, H., Seidman, J.G., and Seidman, C.E. 1995. Familial hypertrophic cardiomyopathy: a genetic model of cardiac hypertrophy. *Hum. Mol. Genet.* **4**:1721–1727.
3. Geisterfer-Lowrance, A.A.T., *et al.* 1996. A mouse model of familial hypertrophic cardiomyopathy. *Science.* **272**:731–734.
4. Watkins, H., *et al.* 1992. Characteristics and prognostic implications of myosin missense mutations in familial hypertrophic cardiomyopathy. *N. Engl. J. Med.* **326**:1108–1114.
5. Srinivasan, S., *et al.* 1998. Noninvasive, *in utero* imaging of mouse embryonic heart development using 40 MHz echocardiography. *Circulation.* **98**:912–918.
6. Aristizabal, O., Christopher, D.A., Foster, F.S., and Turnbull, D.H. 40 MHz echocardiography scanner for cardiovascular assessment of mouse embryos. *Ultrasound Med. Biol.* In press.
7. Lockwood, G.R., Ryan, L.K., Hunt, J.W., and Foster, F.S. 1991. Measurement of the ultrasonic properties of vascular tissues and blood from 35 to 65 MHz. *Ultrasound Med. Biol.* **17**:656–666.
8. McConnell, B.K., Moravec, C.S., and Bond, M. 1998. Troponin-I phosphorylation and myofilament calcium sensitivity during decompensated cardiac failure. *Am. J. Physiol.* **274**:H385–H396.
9. Bland, J.M., and Altman, D.G. 1986. Statistical methods for assessing agreement between two methods of clinical measurement. *Lancet.* **1**:307–310.
10. Lyons, G.E., Schiaffino, S., Sassoon, D., Barton, P., and Buckingham, M. 1990. Developmental regulation of myosin gene expression in mouse cardiac muscle. *J. Cell. Biol.* **111**:2427–2436.
11. Schwartz, K., *et al.* 1981. Myosin isoenzyme distribution correlates with speed of myocardial contraction. *J. Mol. Cell. Cardiol.* **13**:1071–1075.
12. Dorn, G.W., Robbins, J., Ball, N., and Walsh, R.A. 1994. Myosin heavy chain regulation and myocyte contractile depression after LV hypertrophy in aortic-banded mice. *Am. J. Physiol.* **267**:H400–H405.
13. Barany, M. 1967. ATPase activity of myosin correlated with speed of muscle shortening. *J. Gen. Physiol.* **50**(Suppl.):197–218.
14. Pope, B., Hoh, J.F.Y., and Weeds, A. 1980. The ATPase activities of rat cardiac myosin isoenzymes. *FEBS Lett.* **118**:205–208.
15. Lompre, A.M., *et al.* 1981. Species- and age-dependent changes in the relative amounts of cardiac myosin isoenzymes in mammals. *Dev. Biol.* **84**:286–290.
16. Pagani, E.D., and Julian, F.J. 1984. Rabbit papillary muscle myosin isoenzymes and the velocity of muscle shortening. *Circ. Res.* **54**:586–594.
17. Gutgesell, H.P., Paquet, M., Duff, D.F., and McNamara, D.G. 1977. Evaluation of left ventricular size and function by echocardiography. *Circulation.* **56**:457–462.
18. Henry, W.L., Gardin, J.M, and Ware, J.H. 1980. Echocardiographic measurements in normal subjects from infancy to old age. *Circulation.* **62**:1054–1061.
19. St. John Sutton, M.G., Marier, D.L., Oldershaw, P.J., Sacchetti, R., and Gibson, D.G. 1982. Effect of age related changes in chamber size, wall thickness and heart rate on left ventricular function in normal children. *Br. Heart J.* **48**:342–351.
20. Magid, N.M., *et al.* 1988. Hypertrophic and functional response to experimental chronic aortic regurgitation. *J. Mol. Cell. Cardiol.* **20**:239–246.
21. Hoit, B.D., Khoury, S.F., Kranias, E.G., Ball, N., and Walsh, R.A. 1995. In vivo echocardiographic detection of enhanced left ventricular function in gene-targeted mice with phospholamban deficiency. *Circ. Res.* **77**:633–637.
22. Pollick, C., Hale, S.L., and Kloner, R.A. 1995. Echocardiographic and cardiac Doppler assessment of mice. *J. Am. Soc. Echocardiogr.* **8**:602–610.
23. Tanaka, N., *et al.* 1996. Transthoracic echocardiography in models of cardiac disease in the mouse. *Circulation.* **94**:1109–1117.
24. Pawlush, D.G., Moore, R.L., Musch, T.I., and Davidson, W.R. 1993. Echocardiographic evaluation of size, function and mass of normal and hypertrophied rat ventricles. *J. Appl. Physiol.* **74**:2598–2605.

25. Rayment, I., *et al*. 1993. Structure of the actin-myosin complex and its implications for muscle contraction. *Science*. **261**:58–65.
26. Sweeney, H.L., Straceski, A.J., Leinwand, L.A., Tikunov, B.A., and Faust, L. 1994. Heterologous expression of a cardiomyopathic myosin that is defective in its actin interaction. *J. Biol. Chem*. **269**:1603–1605.
27. Sata, M., and Ikebe, M. 1996. Functional analysis of the mutations in the human cardiac β-myosin that are responsible for familial hypertrophic cardiomyopathy. *J. Clin. Invest*. **98**:2866–2873.
28. Cuda, G., Fananapazir, L., Zhu, W.-S., Sellars, J.R., and Epstein, N.D. 1993. Skeletal muscle expression and abnormal function of b-myosin in hypertrophic cardiomyopathy. *J. Clin. Invest*. **91**:2861–2865.
29. Lankford, E.B., Epstein, N.D., Fananapazir, L., and Sweeney, H.L. 1995. Abnormal contractile properties of muscle fibers expressing β-myosin heavy chain gene mutations in patients with hypertrophic cardiomyopathy. *J. Clin. Invest*. **95**:1409–1414.
30. Spindler, M., *et al*. 1998. Diastolic dysfunction and altered energetics in the $\alpha MHC^{403/+}$ mouse model of familial hypertrophic cardiomyopathy. *J. Clin. Invest.* **101**:1775–1783.
31. Gwathmey, J.K., *et al*. 1991. Diastolic dysfunction in hypertrophic cardiomyopathy. *J. Clin. Invest.* **87**:1023–1031.
32. Anderson, H.C. 1983. Calcific diseases. *Arch. Pathol. Lab. Med*. **107**:341–347.
33. Levy, R.J., *et al*. 1983. Biologic determinants of dystrophic calcification and osteocalcin deposition in glutaraldehyde-preserved porcine aortic valve leaflets implanted subcutaneously in rats. *Am. J. Pathol*. **113**:143–155.
34. Topaz, O. 1991. Myocardial calcifications in neonates and infants: a unique tissue reaction. *South. Med. J*. **84**:891–895.
35. Parodi, O., *et al*. 1993. Myocardial blood flow distribution in patients with ischemic heart disease or dilated cardiomyopathy undergoing heart transplantation. *Circulation*. **88**:509–522.
36. Nishi, H., *et al*. 1994. Possible gene dosage effect of a mutant cardiac β-myosin heavy chain gene on the clinical expression of familial hypertrophic cardiomyopathy. *Biochem. Biophys. Res. Commun*. **200**:549–556.
37. Anversa, P., *et al.* 1995. Ischemic cardiomyopathy: myocyte cell loss, myocyte cellular hypertrophy and myocyte cellular hyperplasia. *Ann. NY Acad. Sci*. **752**:47–64.
38. Anversa, P., Zhang, X., Li, P., and Capasso, J.M. 1992. Chronic coronary artery constriction leads to moderate myocyte loss and left ventricular dysfunction and failure in rats. *J. Clin. Invest.* **89**:618–629.
39. Anversa, P., T. Palackal, E.H. Sonnenblick, G. Olivetti, and J.M. Capasso. 1990. Hypertensive cardiomyopathy. *J. Clin. Invest*. **85**:994–997.
40. Spinale, F.G., Zellner, J.L., Tomita, M., Crawford, F.A., and Zile, M.R. 1991. Relation between ventricular and myocyte remodeling with the development and regression of supraventricular tachycardia-induced cardiomyopathy. *Circ. Res*. **69**:1058–1067.
41. Kajsturam, J., *et al.* 1995. The cellular basis of pacing-induced dilated cardiomyopathy. *Circulation*. **92**:2306–2317.
42. Olivetti G., Melissari, M., Capasso, J.M., and Anversa, P. 1991. Cardiomyopathy of the aging human heart. *Circ. Res*. **68**:1560–1568.